Electrochemical surface plasmon resonance measurements of camel-shaped static capacitance and slow dynamics of electric double layer structure at the ionic liquid/electrode interface

AUTHOR(S):

Zhang, Shiwei; Nishi, Naoya; Sakka, Tetsuo

The Journal of Chemical Physics

Electrochemical surface plasmon resonance measurements of camel-shaped static capacitance and slow dynamics of electric double layer structure at the ionic liquid/electrode interface

Cite as: J. Chem. Phys. **153**, 044707 (2020); https://doi.org/10.1063/5.0011671
Submitted: 23 April 2020 . Accepted: 08 July 2020 . Published Online: 28 July 2020

Shiwei Zhang, Naoya Nishi, and Tetsuo Sakka

The Journal of Chemical Physics ARTICLE scitation.org/journal/jcp

Electrochemical surface plasmon resonance measurements of camel-shaped static capacitance and slow dynamics of electric double layer structure at the ionic liquid/electrode interface

Cite as: J. Chem. Phys. 153, 044707 (2020); doi: 10.1063/5.0011671
Submitted: 23 April 2020 • Accepted: 8 July 2020 •
Published Online: 28 July 2020 • Publisher error corrected: 28 July 2020

Shiwei Zhang, Naoya Nishi,[a] and Tetsuo Sakka

AFFILIATIONS

Department of Energy and Hydrocarbon Chemistry, Graduate School of Engineering, Kyoto University, Kyoto 615-8510, Japan

[a]Author to whom correspondence should be addressed: nishi.naoya.7e@kyoto-u.ac.jp

ABSTRACT

Electrochemical surface plasmon resonance (ESPR) is applied to evaluate the relative static differential capacitance at the interface between 1-butyl-3-methylimidazolium bis(trifluoromethanesulfonyl)amide ionic liquid (IL) and a gold electrode, based on the relationship between the SPR angle and surface charge density on the electrode. Potential-step and potential-scan ESPR measurements are used to probe the dynamics of the electric double layer (EDL) structure that exhibit anomalously slow and asymmetrical characteristics depending on the direction of potential perturbation. EDL dynamics respond at least 30 times more slowly to changes of potential in the positive direction than in the negative direction. ESPR experiments with the positive-going potential scan are significantly affected by the slow dynamics even at a slow scan. The surface charge density that reflects the relative static capacitance is obtained from the negative-going potential scans. The evaluated quasi-static differential capacitance exhibits a camel-shaped potential dependence, thereby agreeing with the prediction of the mean-field lattice gas model of the EDL in ILs. ESPR is shown to be an effective experimental method for determining relative values of the static differential capacitance.

I. INTRODUCTION

Ionic liquids (ILs), which are new materials exhibiting flame resistance, low volatility,[1,2] and high thermal/electrochemical stability,[3,4] have garnered attention as electrolytes for electrochemical devices, such as supercapacitors[5,6] and batteries.[7,8] The electric double layer (EDL) at the electrolyte/electrode interface affects the performance of energy devices involved with electrode reactions (redox reactions) and charging processes. The structure and dynamics of ILs within the EDL are significantly different from those of conventional electrolytes. The ionic distribution in the EDL at the IL/electrode interface cannot be described by the conventional Gouy–Chapman–Stern model. In theoretical studies conducted by Kornyshev *et al.*,[9–11] a mean-field lattice gas model was proposed to predict the ionic distribution and differential capacitance. These properties have been examined in simulation studies of the EDL structure of ILs.[12–17] Electrochemical impedance spectroscopy (EIS) is the most popular experimental method for evaluating the differential capacitance at the IL/electrode interface.[18–20] In numerous studies, the slow dynamics of the EDL structure of ILs, such as ultraslow relaxation[19,21–25] and hysteresis,[18,26–30] have been revealed. The typical ac potential oscillation in EIS measurements is faster than the slow EDL dynamics, making EIS unsuitable to evaluate the static capacitance for comparison with theoretical predictions. Therefore, we have used the pendant-drop method, which measures the interfacial tension at equilibrium and experimentally

provides the static differential capacitance.[31,32] However, a liquid–liquid interface must be used in the pendant-drop method, limiting the electrode materials to liquids, such as mercury[31,32] and GaIn alloy.[33]

Electrochemical surface plasmon resonance (ESPR) can be used to detect variations in interfacial structure with respect to a change in potential because the SPR angle is sensitive to the local refractive index around the interface between the dielectric medium and the metal film.[34,35] In our previous studies, ESPR proved to be an effective probe of ultraslow relaxation[23] and redox reactions[36] at the IL/gold interface. In this study, we have presented the prospect that the static differential capacitance at the solid electrode/IL interface can be obtained using ESPR. A relationship between the SPR angle and the surface charge density at the IL/electrode interface has been established. Owing to this relationship, the surface charge density has been determined through the variation in SPR angle measured during potential-scan and potential-step experiments. If the potential perturbation is sufficiently slow compared with the EDL dynamics, the quasi-static differential capacitance of the EDL at the IL/gold interface can be obtained. The effects of potential scan rate and direction on the slow IL dynamics have been investigated in detail.

II. MODEL

We consider a Kretschmann system with a prism/thin metal film/dielectric medium interface, where the light coming from the prism side of the interface undergoes total internal reflection. SPR occurs at an incident angle where the wavenumber of the surface plasmon wave is matched by that of the tangential surface component of the evanescent wave generated by total internal reflection. The incidence angle under that condition, which is the SPR angle, θ_{SPR}, is represented in terms of the refractive indexes of the metal film, n_m, dielectric medium, n_d, and prism, n_p, as expressed by the following equation:[37]

$$\theta_{SPR} = \sin^{-1}\left(\frac{1}{n_p}\sqrt{\frac{1}{1/\mathrm{Re}(n_m{}^2) + 1/n_d{}^2}}\right). \tag{1}$$

Wang *et al.*[38] proposed a phenomenological model as the basic ESPR formalism in which the variation of the SPR angle, $\Delta\theta_{SPR}$, is written as the sum of two parts. One part is the change in surface charge density on the electrode, which results in a small variation of n_m on the surface. The second part comprises the reactant and product concentration changes driven by an electrode reaction. For the prism/gold film/IL interface system in this study, the dielectric medium is an IL with an ion concentration on the order of mol dm^{-3} and no redox species. In this case, the change in ion concentration in the EDL should also contribute to the change in n_d, which was neglected in the previous study[38] because the ion concentration in a typical electrolyte solution is relatively low. In the present study, we presume that the second contribution to the change in SPR angle is given by the change in ion concentrations. Hence, $\Delta\theta_{SPR}$ is expressed as

$$\begin{aligned}\Delta\theta_{SPR} &= \Delta\theta_q + \Delta\theta_{ic} \\ &= A\Delta q_M + B\int_0^\infty [\alpha_c\Delta c_c(z) + \alpha_a\Delta c_a(z)]e^{-\frac{z}{l}}\,d(z/l).\end{aligned} \tag{2}$$

In Eq. (2), the change in the SPR angle, $\Delta\theta_{SPR}$, is the sum of the following parts: $\Delta\theta_q$, which is caused by the change in the surface charge density on the gold film (Δq_M), and $\Delta\theta_{ic}$, which is caused by the change in the cation and anion concentrations in the EDL (Δc_c and Δc_a, respectively). The proportionality constants A, B, α_c, and α_a are written as

$$\begin{aligned}A &= \left.\frac{\partial\theta}{\partial q_M}\right|_{\theta=\theta_{SPR}}, \quad B = \left.\frac{\partial\theta}{\partial n_d}\right|_{\theta=\theta_{SPR}}, \\ \alpha_c &= \left.\frac{\partial n_d}{\partial c_c}\right|_{c_c=c_{IL}}, \quad \alpha_a = \left.\frac{\partial n_d}{\partial c_a}\right|_{c_a=c_{IL}}.\end{aligned} \tag{3}$$

B is calculated using Eq. (1), whereas α_c and α_a are calculated from the Lorentz–Lorenz equation given as follows:[39,40]

$$\frac{n_d{}^2 - 1}{n_d{}^2 + 2} = \frac{N_A(p_a c_a + p_c c_c)}{3\varepsilon_0}, \tag{4}$$

where p_i is the mean polarizability of the ions, N_A is the Avogadro constant, and ε_0 is the vacuum permittivity. The variable z in Eq. (2) is the displacement in the IL normal to the surface of the gold film ($z = 0$).

The change in n_d near the interface reflects the change in ion concentration in the EDL thickness of δ_{EDL}, which is on the order of nm. This distance is significantly smaller than the decay length, l, of the evanescent field from the interface into the IL bulk, which is on the order of 100 nm. The decay length of the evanescent wave is calculated by using the following equation:[37]

$$l = \left(\mathrm{Im}\left[\frac{2\pi n_d}{\lambda}\sqrt{1 - \left(\frac{n_p \sin\theta_{SPR}}{n_d}\right)^2}\right]\right)^{-1}. \tag{5}$$

Therefore, even if the distribution of ion concentrations is assumed to be uniform within the EDL, changes in the local n_d have little influence on the calculated result. Assuming that Δc_a changes proportionally to Δc_c with a negative coefficient, β, when q_M changes, we can write the concentration changes, Δc_c and Δc_a, as in the following equation:

$$\Delta c_a = \beta\Delta c_c = \frac{\Delta q_M}{(1 - \beta^{-1})\delta_{EDL}F}, \tag{6}$$

where F is the Faraday constant. Although β is potential dependent, it is considered to be constant in the narrow interval around the potential of zero charge (E_{pzc}). This leads to the following equation for $\Delta\theta_{ic}$:

$$\Delta\theta_{ic} = B(\alpha_c + \beta\alpha_a)\left(1 - e^{-\frac{\delta_{EDL}}{l}}\right)\frac{\Delta q_M}{(\beta - 1)\delta_{EDL}F}. \tag{7}$$

The following limit is valid with respect to δ_{EDL}/l:

$$\lim_{\frac{\delta_{EDL}}{l}\to 0}\frac{1 - e^{-\frac{\delta_{EDL}}{l}}}{\frac{\delta_{EDL}}{l}} = 1. \tag{8}$$

Given all assumptions above, $\Delta\theta_{SPR}$ depends only on a single experimental variable, Δq_M, as shown in the following equation:

$$\Delta\theta_{SPR} = \Delta q_M \left[A + B\frac{\alpha_c + \beta\alpha_a}{(\beta - 1)lF} \right]. \quad (9)$$

Thus, Δq_M can be obtained from $\Delta\theta_{SPR}$ in an ESPR potential-scan measurement. The differential capacitance, C_d, is calculated as

$$C_d = \frac{dq_M}{dE} = X\frac{d\theta_{SPR}}{dE},$$
$$X = \left[A + B\frac{\alpha_c + \beta\alpha_a}{(\beta - 1)lF} \right]^{-1}. \quad (10)$$

Concerning the quantitative calculation, it is difficult to precisely evaluate coefficient A. The Drude model,[41,42] which establishes the relationship between q_M and n_m, can be used to evaluate A, but only semiquantitatively. Foley *et al.*[43] proposed A equal to 0.021 deg·m^2·C^{-1} for the gold/electrolyte solution interface based on surface impedance measurements, where the SPR response was measured under an ac potential perturbation. However, the value is not applicable to other systems comprising different electrolytes, metals, and metal film thicknesses. Moreover, application of an ac potential is unsuitable for IL systems due to their slow dynamics. Therefore, surface impedance measurements are not applicable here. Another way to evaluate A is to use the Hansen method,[44] which allows the light reflectivity of multilayer systems to be determined. The metal film in this study is approximated as a bilayer comprising a "bulk" film layer and a thin surface layer of several angstroms thickness on the metal film, whose free electron density varies with q_M.[45] There is no reliable method to determine the thickness of the surface layer precisely, which affects the calculated result. In the present study, the linear relationship between $\Delta\theta_{SPR}$ and Δq_M is sufficient to consider the potential dependence of the static differential capacitance at the solid electrode interface of an IL. We use C_dX^{-1} rather than the absolute value of C_d in discussing the potential dependence of C_d. Although the exact value of A is not necessary, it remains an important future research objective. For example, molecular dynamics (MD) simulation would be helpful in evaluating A, α, and β.

III. EXPERIMENTAL

1-Butyl-3-methylimidazolium bis(trifluoromethanesulfonyl)-amide ([C$_4$mim$^+$][TFSA$^-$]) was chosen as the IL, which was prepared from synthesized[46] [C$_4$mim$^+$]Cl$^-$ and purchased Li$^+$[TFSA$^-$] (Kanto Chemical) and purified according to the procedure reported previously.[47] An SPR instrument (Springle, Kinetic Evaluation Instruments) with a Kretschmann configuration[48] was used as in our previous works.[23,36] The IL was vacuum evacuated for more than 2 h before measurement to avoid the effect of impurities. The working electrode (WE) was a 50-nm gold film deposited on a SF15 glass (refractive index = 1.6911 at 670 nm). The electrode was cleaned with Piranha solution. A 670-nm laser beam illuminated the IL-covered gold film in an atmosphere of Ar gas (99.9%) at room temperature. The refractive indexes of gold, 0.174 + 3.612i, and [C$_4$mim$^+$][TFSA$^-$], 1.434, at 670 nm were taken from the literature[49] and spectroscopic ellipsometry of the IL surface,[50] respectively. The WE surface area was 7.1 × 10^{-2} cm^2. An AgCl-coated Ag wire quasi-reference electrode (QRE) and a Pt wire counter electrode were inserted directly into the IL. Due to the high viscosity of the IL, the small amounts of Ag$^+$ and Cl$^-$ released from the QRE likely remain near the AgCl surface and scarcely diffuse to the WE within the experimental time scale. Thus, the QRE potential is relatively stable. The WE potential with respect to the QRE was controlled by a PC-controlled potentiostat (Autolab Type III). The shift of the SPR angle, $\Delta\theta_{SPR}$, from that at $t = 0$ was recorded during the measurements.

IV. RESULTS AND DISCUSSION

The SPR angles obtained at three cyclic scan rates are shown in Fig. 1. The $\Delta\theta_{SPR}$ vs E plots are sigmoidal in shape with the largest slope occurring at the potential of zero charge, $E_{pzc} = -0.61$ V, which was evaluated from the Fc/Fc$^+$ redox potential in this system (Fig. S1 in the supplementary material) and the reported E_{pzc} vs Fc/Fc$^+$ at the [C$_4$mim$^+$][TFSA$^-$]/gold interface.[27] The SPR angle on the negative scan is nearly constant at potentials far removed from E_{pzc} but changes dramatically near E_{pzc} when scanning from 0 V to −1.2 V. The current recorded concurrently [Fig. S2(a) in the supplementary material] shows a peak during the negative scan in this potential range. The position of the current peak indicates that a large change in surface charge accompanies the variation in SPR angle, which may reflect the EDL charging process. However, residual faradaic processes cannot be completely excluded in these experiments, as will be discussed below. The total change in $\Delta\theta_{SPR}$ on the forward negative scan (0 V → −1.8 V) is almost the same for all three scan rates, whereas the change on the −1.8 V → +1 V positive scan decreases gradually with increasing scan rate. We presume that the asymmetry of the ultra-slow relaxation is the cause of this behavior, as we have reported for another IL.[23] The ultra-slow relaxation prevents measurement of the static capacitance. However, Fig. 1 shows that relaxation occurs rapidly on the negative-going scan, which indicates its possible use for evaluating the static capacitance.

Potential-step ESPR measurements were performed to confirm EDL relaxation at the [C$_4$mim$^+$][TFSA$^-$]/gold interface. According

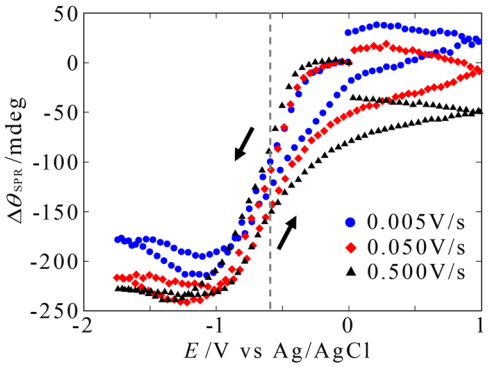

FIG. 1. Variation of the SPR angle during cyclic potential scans at three scan rates. Each potential scan begins at 0 V and proceeds to negative values. The vertical dashed line indicates the potential of zero charge ($E_{pzc} = -0.61$ V).

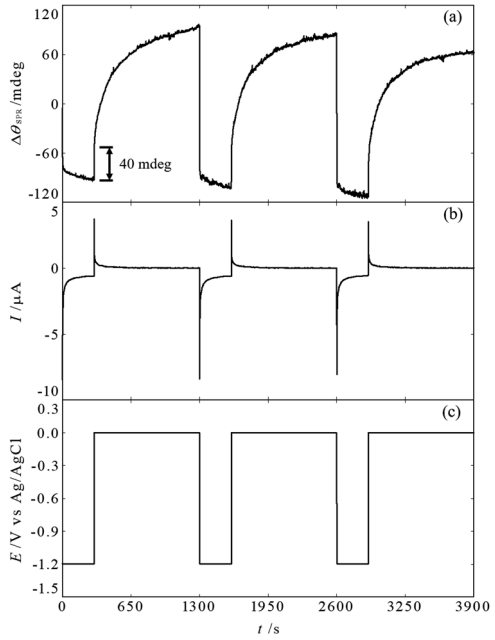

FIG. 2. SPR angle (a) and current (b) changes following multi potential steps (c) in which the potential is held at 0 V for 1000 s and at −1.2 V for 300 s.

to the mean-field lattice gas model for ionic-liquid EDLs, the potential dependence of C_d near E_{pzc} shows the characteristic bell-shaped or camel-shaped curves instead of the U-shaped curve of dilute electrolytes.[9–11] Therefore, all experiments were conducted relative to the E_{pzc} (−0.61 V) with step-potential limits symmetrically chosen to be 0 V and −1.2 V.

The results of multiple potential-step measurements are shown in Fig. 2. The potential was held at 0 V for 1000 s and at −1.2 V for 300 s. The SPR angle and current results confirm that the asymmetric dynamics of the system depend on the direction of the potential step. On the 0 → −1.2 V step, the SPR angle decreases rapidly by more than 160 mdeg and is accompanied almost instantaneously by a large increase in negative current, after which $\Delta\theta_{SPR}$ decreases by less than 20 mdeg over 300 s. On the −1.2 → 0 V step, the SPR angle increases by less than 40 mdeg and is accompanied by a smaller increase in positive current. As the potential is held at 0 V for 1000 s, the angle slowly increases by 120 mdeg.

The charge obtained by integrating the current is shown in Fig. S3 of the supplementary material. The stable current after relaxation is attributed to the faradaic current, the accumulation of which should not be included in the surface charge at the electrode interface. The charges evaluated by integration of the current in Figs. S2 and S3 differ significantly in appearance from the variations in the SPR angle. The evaluated charge is always large and negative, which demonstrates that it does not correspond to Δq_M. Therefore, Δq_M cannot be evaluated, even in a relative sense, by the current recorded in electrochemical measurements. The experimental current is considerably sensitive to impurities such as water and oxygen. Small amounts of impurities are easily detected as faradaic current but do not cause a change in the refractive index because they diffuse beyond the evanescent field layer and do not accumulate in the EDL. Thus, ESPR is a powerful means of monitoring Δq_M, which is difficult by CV.

Figure 3 shows single-graph overlays from Fig. 2 of the three relaxation curves obtained following negative and positive potential steps. There is a small difference in response following the first negative step [Fig. 3(a)] in that the excursion of $\Delta\theta_{SPR}$ is smaller than that following the subsequent potential steps. Considering that the first negative step begins from a completely relaxed state, it is reasonable that the SPR angle response differs slightly from that of steps starting from a state in the middle of the relaxation. Similar asymmetric relaxation dynamics have been reported at a gold interface with trioctylmethylammonium bis(nonafluorobutanesulfonyl)amide [$TOMA^+$][$C_4C_4N^-$].[23] According to Ref. 23, the direction of the rapid $\Delta\theta_{SPR}$ shift is opposite to that of the potential step because the large polar $TOMA^+$ and $C_4C_4N^-$ ions readily undergo electronic and rotational polarization when the potential changes.[23] However, the SPR angle responses of [C_4mim^+][$TFSA^-$] are always in the same direction as the potential step and thus differ from the behavior of [$TOMA^+$][$C_4C_4N^-$]. A possible explanation is that C_4mim^+ and $TFSA^-$ possess more localized charge distributions, because of their smaller ionic volumes. Hence, their relatively small electronic and rotational polarizations are negligible.

The potential step measurements indicate that the relaxation dynamics of [C_4mim^+][$TFSA^-$] are at least 30 times slower in the positive than in the negative direction. The relatively rapid response of $\Delta\theta_{SPR}$ to a negative potential step means that the entire relaxation process is almost completed within a very short time [Fig. 3(a)].

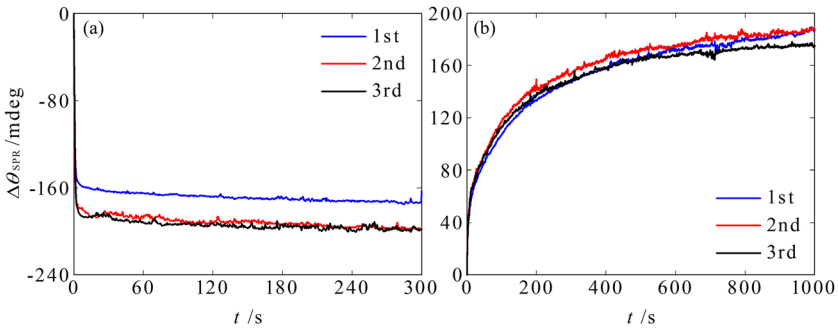

FIG. 3. SPR angle response following the three successive negative (a) and positive (b) potential steps in Fig. 2.

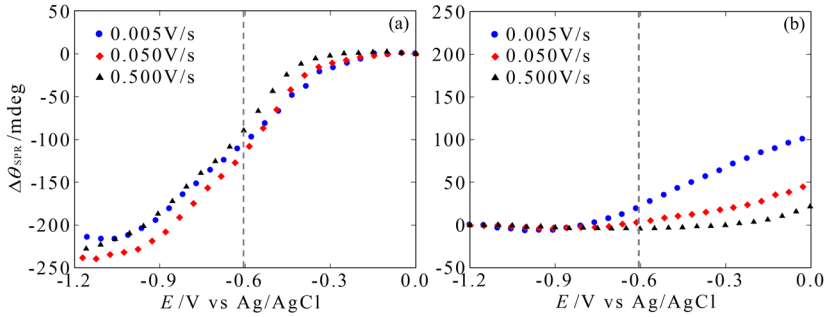

FIG. 4. SPR angle changes upon negative (a) and positive (b) linear potential scans at three scan rates.

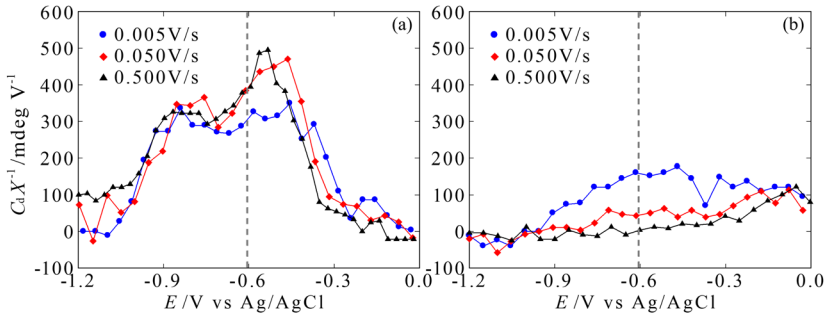

FIG. 5. Capacitance plots evaluated from SPR angles obtained on negative-going (a) and positive-going (b) potential scans.

In the model section, we described the proportionality of $\Delta\theta_{SPR}$ to Δq_M without considering the slow dynamics [Eq. (9)]. Therefore, the quasi-static C_d is calculated from Eq. (10) using negative potential scan results. Figure 4 shows the changes in $\Delta\theta_{SPR}$ observed upon linear potential scans in the negative (a) and positive (b) directions. All measurements began after a hold at the initial potential for at least 1000 s. The linear potential scans were performed in each direction at three different scan rates. The results from the 0.005 V/s scan rate are at the lower limit for obtaining reliable data unaffected by the drift of the SPR angle.

The potential dependences of $\Delta\theta_{SPR}$ are almost independent of scan rate for the negative scan in Fig. 4(a). However, $\Delta\theta_{SPR}$ is more strongly influenced by the scan rate in the positive scans shown in Fig. 4(b), where faster scan rates produce smaller shifts of $\Delta\theta_{SPR}$. As discussed on the potential-step measurements (Figs. 2 and 3), relaxation processes are negligible for potential changes in the negative direction but are significant for potential changes in the positive direction. The linear potential-scan measurements highlight the fact that the dynamical asymmetry is related only to the direction of potential change not to a specific range of potentials.

Figures 5(a) and 5(b) show C_d results obtained from negative [Fig. 4(a)] and positive [Fig. 4(b)] linear potential scans, respectively, using Eq. (10). The y-axis in Fig. 5 is C_d/X [see Eq. (10)]. As expected, the capacitance shown in Fig. 5(a) obtained on negative scan is only slightly influenced by scan rate, whereas that obtained on positive scan [Fig. 5(b)] is significantly affected. Values of C_d in Fig. 5(b) are considerably lower than those in Fig. 5(a) and decrease completely at the larger scan rates. The results are consistent with slow dynamics following a positive change in potential [Fig. 3(b) for potential step and Fig. 4(b) for potential scan]. C_d is calculated to be a negative number at several potentials, which is physically impossible. The phenomenon is comparable to the static C_d results obtained by the pendant drop method,[31] where the $[C_2mim^+][BF_4^-]$ and $[C_8mim^+][BF_4^-]$ ILs exhibit static C_d values of near 0 at both the extremes of their bell-shaped or camel-shaped C_d curves. The $[C_4mim^+][TFSA^-]$ results in the present study support this observation; however, according to the sigmoidal-shape of the $\Delta\theta_{SPR}$ response in Fig. 1, C_d does not increase at potentials far from E_{pzc}, unlike the behavior in Ref. 31.

The potential dependence of the differential capacitance illustrated in Fig. 5(a) as a camel-shaped response centered at the E_{pzc}

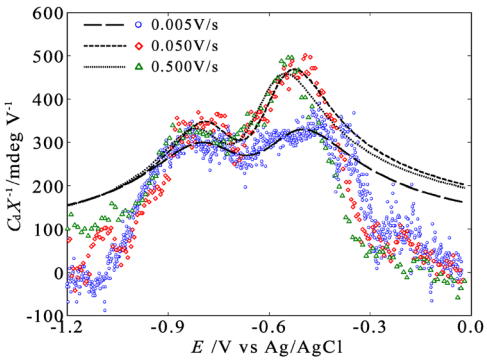

FIG. 6. Capacitance values (points) determined from SPR angles obtained on negative-going potential scans and curves (dashed lines) fitted to the mean-field lattice gas model.

TABLE I. Parameters fitted using the mean-field lattice gas model.

Scan rate (V/s)	ΔE_{fit} (V)	$C_{d0}X^{-1}$ (mdeg/V)	α	γ_a	γ_c	E_{pzc} (V)
0.005	−0.965 to −0.327	402 ± 8	0.451 ± 0.012	0.157 ± 0.005	0.211 ± 0.008	−0.667 ± 0.004
0.050	−0.894 to −0.400	394 ± 13	0.60 ± 0.02	0.091 ± 0.005	0.199 ± 0.013	−0.688 ± 0.005
0.500	−0.947 to −0.473	390 ± 20	0.59 ± 0.04	0.089 ± 0.006	0.212 ± 0.023	−0.719 ± 0.007

appears to be a universal observation. The behavior is relatively well explained by the mean-field lattice gas model,[9–11] which was used to fit the C_d data from Fig. 5(a) by means of the following equation:[10]

$$C_d = C_{d0}\frac{\cosh(\alpha u/2)}{1+2\gamma(u)\sinh^2(\alpha u/2)}\sqrt{\frac{2\gamma(u)\sinh^2(\alpha u/2)}{\ln\left[1+2\gamma(u)\sinh^2(\alpha u/2)\right]}},$$
$$\gamma(u) = \gamma_a + \frac{\gamma_a-\gamma_c}{1+e^{\alpha u}}, \tag{11}$$
$$u = \frac{(E-E_{pzc})F}{RT},$$

where C_{d0} is the differential capacitance at E_{pzc} (fitted together with the coefficient X as one parameter), α is a short-range correlation parameter arising from the difference between the attraction of counterions and repulsion of co-ions, γ_a and γ_c are the compacity parameters, which equal the ratio of the bulk to maximum concentration of anions and cations, respectively, in the EDL, R is the gas constant, and T is the temperature. According to the pendant drop experiments[31,32] and molecular dynamics (MD) simulations,[16,17] application of the mean-field lattice gas model is limited to potentials close to the E_{pzc} because factors such as the reorientation and densification of ions in the EDL are not included in the model. The potential range of fitted data in this study, ΔE_{fit}, was chosen to minimize the deviation of the data from the fitted curves and to extend as widely as possible around the E_{pzc}. The fitted curves at different scan rates are shown in Fig. 6, and the fitted parameters with standard errors are found in Table I.

The fitted values of $C_{d0}X^{-1}$ decrease slightly and the potential of zero charge, E_{pzc}, moves in the negative direction as the scan rate increases. Both observations demonstrate that the slow dynamics are non-negligible even in the negative potential scan. γ_a is smaller than γ_c at all three scan rates. This difference causes the C_d maximum to be larger on the positive side of the E_{pzc} based on the mean-field lattice gas model with asymmetric ionic sizes.[51] This characteristic was also observed in MD simulation studies on the $[C_4mim^+][TFSA^-]$/graphite interface.[52,53] The values of γ_c are almost constant (~0.2), whereas those of γ_a decrease with increasing scan rate. Thus, cation dynamics may be faster than anion dynamics, which could be the apparent origin of the slow dynamics that occur when the potential is changed in the positive direction.

V. CONCLUSIONS

In the present study, we propose a phenomenological model for measuring the static differential capacitance at a solid electrode/IL interface using ESPR. The change in the SPR angle, $\Delta\theta_{SPR}$, is expressed as a product of the change in surface charge density and a coefficient based on characteristic responses of refractive indexes at the interface to the change in surface charge density. Experimental validation was performed by potential-scan ESPR measurements at the gold/$[C_4mim^+][TFSA^-]$ interface. The resulting plots of $\Delta\theta_{SPR}$ vs potential are sigmoidal in shape. Potential-step experiments were conducted to evaluate the effects of slow dynamics at the IL/gold interface. Asymmetrical dynamics, which depend on the direction of potential change, are observed for $[C_4mim^+][TFSA^-]$. The dynamics following a negative potential change are significantly faster than a positive potential change. The SPR angle results obtained by linear potential scan in different directions and at different scan rates agree with potential-step results. The asymmetry depends only on the direction of potential change and not the range of potential values. Quasi-static differential capacitances calculated from the SPR angle changes on negative potential scan show camel-shaped curves without significant dynamical effects and agree with the mean-field lattice gas model[9–11] and MD simulation results.[52,53] More detailed studies of interfacial IL dynamics by ESPR are in progress.

SUPPLEMENTARY MATERIAL

See the supplementary material for the evaluation of the potential of zero charge in the system and the current results recorded in the ESPR experiments.

ACKNOWLEDGMENTS

This work was partly supported by JSPS KAKENHI (Grant No. 18K05171) and Kato Foundation for Promotion of Science.

DATA AVAILABILITY

The data that support the findings of this study are available from the corresponding author upon reasonable request.

REFERENCES

[1] Y. Rosenfeld, J. Chem. Phys. **98**, 8126 (1993).
[2] M. J. Earle, J. M. S. S. Esperança, M. A. Gilea, J. N. Canongia Lopes, L. P. N. Rebelo, J. W. Magee, K. R. Seddon, and J. A. Widegren, Nature **439**, 831 (2006).
[3] M. Galiński, A. Lewandowski, and I. Stępniak, Electrochim. Acta **51**, 5567 (2006).
[4] A. Lewandowski and A. Świderska-Mocek, J. Power Sources **194**, 601 (2009).
[5] C. Zhong, Y. Deng, W. Hu, J. Qiao, L. Zhang, and J. Zhang, Chem. Soc. Rev. **44**, 7484 (2015).
[6] T. Y. Kim, H. W. Lee, M. Stoller, D. R. Dreyer, C. W. Bielawski, R. S. Ruoff, and K. S. Suh, ACS Nano **5**, 436 (2011).

[7]R. Lin, P.-L. Taberna, S. Fantini, V. Presser, C. R. Pérez, F. Malbosc, N. L. Rupesinghe, K. B. K. Teo, Y. Gogotsi, and P. Simon, J. Phys. Chem. Lett. **2**, 2396 (2011).
[8]V. Borgel, E. Markevich, D. Aurbach, G. Semrau, and M. Schmidt, J. Power Sources **189**, 331 (2009).
[9]A. A. Kornyshev, J. Phys. Chem. B **111**, 5545 (2007).
[10]Z. A. H. Goodwin, G. Feng, and A. A. Kornyshev, Electrochim. Acta **225**, 190 (2017).
[11]Z. A. H. Goodwin and A. A. Kornyshev, Electrochem. Commun. **82**, 129 (2017).
[12]M. V. Fedorov and A. A. Kornyshev, Electrochim. Acta **53**, 6835 (2008).
[13]M. V. Fedorov, N. Georgi, and A. A. Kornyshev, Electrochem. Commun. **12**, 296 (2010).
[14]J. Vatamanu, O. Borodin, and G. D. Smith, J. Am. Chem. Soc. **132**, 14825 (2010).
[15]M. Chen, Z. A. H. Goodwin, G. Feng, and A. A. Kornyshev, J. Electroanal. Chem. **819**, 347 (2018).
[16]S. Katakura, N. Nishi, K. Kobayashi, K. Amano, and T. Sakka, Phys. Chem. Chem. Phys. **22**, 5198 (2020).
[17]S. Katakura, N. Nishi, K. Kobayashi, K. Amano, and T. Sakka, J. Phys. Chem. C **124**, 7873 (2020).
[18]V. Lockett, R. Sedev, J. Ralston, M. Horne, and T. Rodopoulos, J. Phys. Chem. C **112**, 7486 (2008).
[19]R. Atkin, N. Borisenko, M. Drüschler, F. Endres, R. Hayes, B. Huber, and B. Roling, J. Mol. Liq. **192**, 44 (2014).
[20]J. M. Klein, E. Panichi, and B. Gurkan, Phys. Chem. Chem. Phys. **21**, 3712 (2019).
[21]M. Chu, M. Miller, T. Douglas, and P. Dutta, J. Phys. Chem. C **121**, 3841 (2017).
[22]A. Rahman, M. M. Rahman, M. Y. A. Mollah, and M. A. B. H. Susan, J. Phys. Chem. B **123**, 5577 (2019).
[23]N. Nishi, Y. Hirano, T. Motokawa, and T. Kakiuchi, Phys. Chem. Chem. Phys. **15**, 11615 (2013).
[24]S. Makino, Y. Kitazumi, N. Nishi, and T. Kakiuchi, Electrochem. Commun. **13**, 1365 (2011).
[25]Y. Yasui, Y. Kitazumi, R. Ishimatsu, N. Nishi, and T. Kakiuchi, J. Phys. Chem. B **113**, 3273 (2009).
[26]W. Zhou, S. Inoue, T. Iwahashi, K. Kanai, K. Seki, T. Miyamae, D. Kim, Y. Katayama, and Y. Ouchi, Electrochem. Commun. **12**, 672 (2010).
[27]K. Motobayashi, K. Minami, N. Nishi, T. Sakka, and M. Osawa, J. Phys. Chem. Lett. **4**, 3110 (2013).
[28]K. Motobayashi, N. Nishi, Y. Inoue, K. Minami, T. Sakka, and M. Osawa, J. Electroanal. Chem. **800**, 126 (2017).
[29]A. Uysal, H. Zhou, G. Feng, S. S. Lee, S. Li, P. Fenter, P. T. Cummings, P. F. Fulvio, S. Dai, J. K. McDonough, and Y. Gogotsi, J. Phys. Chem. C **118**, 569 (2014).
[30]N. Nishi, K. Minami, K. Motobayashi, M. Osawa, and T. Sakka, J. Phys. Chem. C **121**, 1658 (2017).
[31]N. Nishi, A. Hashimoto, E. Minami, and T. Sakka, Phys. Chem. Chem. Phys. **17**, 5219 (2015).
[32]N. Nishi, S. Yasui, A. Hashimoto, and T. Sakka, J. Eletroanal. Chem. **789**, 108 (2017).
[33]N. Nishi, Y. Kojima, S. Katakura, and T. Sakka, Electrochemistry **86**, 38 (2018).
[34]F. Mirkhalaf and D. J. Schiffrin, J. Electroanal. Chem. **484**, 182 (2000).
[35]X. Yao, J. Wang, F. Zhou, J. Wang, and N. Tao, J. Phys. Chem. B **108**, 7206 (2004).
[36]N. Nishi, Y. Ikeda, and T. Sakka, J. Electroanal. Chem. **817**, 210 (2018).
[37]H. Raether, *Surface Plasmons on Smooth and Rough Surfaces and on Gratings* (Springer, Berlin, 1988).
[38]S. Wang, X. Huang, X. Shan, K. J. Foley, and N. Tao, Anal. Chem. **82**, 935 (2010).
[39]L. Lorenz, Ann. Phys. Chem. **247**, 70 (1880).
[40]H. A. Lorentz, Ann. Phys. Chem. **245**, 641 (1880).
[41]P. Drude, Ann. Phys. **306**, 566 (1900).
[42]P. Drude, Ann. Phys. **308**, 369 (1900).
[43]K. J. Foley, X. Shan, and N. J. Tao, Anal. Chem. **80**, 5146 (2008).
[44]W. N. Hansen, J. Opt. Soc. Am. **58**, 380 (1968).
[45]J. D. E. McIntyre, Surf. Sci. **37**, 658 (1973).
[46]N. Nishi, J. Uchiyashiki, R. Oogami, and T. Sakka, Thin Solid Films **571**, 735 (2014).
[47]M. J. Earle, C. M. Gordon, N. V. Plechkova, K. R. Seddon, and T. Welton, Anal. Chem. **79**, 758 (2007).
[48]E. Kretschmann and H. Raether, Z. Naturforsch., A **23**, 2135 (1968).
[49]A. Rakić, A. Djurišić, J. Elazar, and M. Majewski, Appl. Opt. **37**, 5271 (1998).
[50]N. Nishi, K. Kasuya, and T. Kakiuchi, J. Phys. Chem. C **116**, 5097 (2012).
[51]Y. Han, S. Huang, and T. Yan, J. Phys.: Condens. Matter **26**, 284103 (2014).
[52]J. Vatamanu, O. Borodin, D. Bedrov, and G. D. Smith, J. Phys. Chem. C **116**, 7940 (2012).
[53]Z. Hu, J. Vatamanu, O. Borodin, and D. Bedrov, Electrochim. Acta **145**, 40 (2014).